

FORSETI Overview

Andy Oakey¹, Matt Grote¹, Aliaksei Pilko¹, Alex Blakesley², Jakub Krol²

¹University of Southampton; ²University College London

Freight Optimisation with RiSk and mixed-mode Transport Integration

Inspired by the Nordic god of justice, public judgment, mediation, and reconciliation.

This document provides an outline of the FORSETI model. The concepts and methods are the intellectual property of the e-Drone consortium and should not be reproduced without permission. e-Drone is funded by the Engineering and Physical Sciences Research Council under grant number EP/V002619/1.

1 INTRODUCTION

The Freight Optimisation with RiSk and mixed-mode Transport Integration (FORSETI) is a logistics planning tool, designed to analyse a given situation regarding demand for transport of goods and determine how best to deploy and integrate transport resources to meet that demand. Developed with the collection of NHS diagnostic specimens in mind, it can be used tactically (i.e., short notice, planning for a near future demand), or strategically (i.e., long-term planning, using historic data).

The logistics transport modes available in FORSETI are diesel or electric vans; bicycle couriers; and uncrewed aerial vehicles (UAVs; commonly known as drones or Uncrewed Aircraft Systems, UAS). FORSETI has been developed around the case study of NHS pathology logistics, where samples are taken from patients at doctors' surgeries and transported to centralised pathology laboratories (typically located at large hospitals) for analysis. The underlying framework of FORSETI could easily be applied to other logistics operations through adaptation to the software.

2 SYSTEM STRUCTURE

FORSETI is made up of four component tools that integrate with each other but can also be used independently (Figure 1).

The first is the Land-Energy-Route-Optimiser (LERO), which takes a given origin-destination (OD) pair and identifies (i) the most likely best route between the two sites (supported by the Google API); and (ii) calculates the energy requirements for the connection, based on a statistical correction of the COPERT environmental model using recorded vehicle energy data captured in the Southampton area.

The second is a ground risk optimisation model (GRO), which calculates the best flight trajectory between each OD pair with respect to third-party ground risk. It aims to minimise the cumulative risk over the trajectory to reduce the probability of fatalities in the event of a drone failure. Failures are modelled with either a ballistic, glide, or parachute descent, depending on the drone characteristics; meanwhile, the probability of hitting a third-party and causing a fatality is based on the drone’s state at the point of failure, its energy on impact, wind conditions, and a statistical distribution of the population on the ground, according to census data. Risk optimal trajectories tend to avoid areas of high population density as a result.

The third OD tool is the air energy route optimiser (AERO), which produces energy optimal trajectories, based on the characteristics of the drone and constraints around its speed and control surfaces. Energy optimal trajectories are typically a straight line, following a bell-shaped curve for altitude. In FORSETI, AERO and GRO are used in combination to produce trajectories that are balanced between energy and risk, resulting in paths that are typically an intermediate of straight-line and avoiding high density areas.

The final tool is the Land-Air Logistics Optimiser (LALO), which uses the complete set of OD pair data to analyse the best combination of vans, drones, and cyclists to serve the input demand. Optimising to minimise a balance of operating cost, emissions, and the maximum in-transit time, LALO uses constraints relating to drone site suitability, operator:drone ratios, operating times, and vehicle capacities.

The remainder of this document outlines how each component of FORSETI functions in more depth.

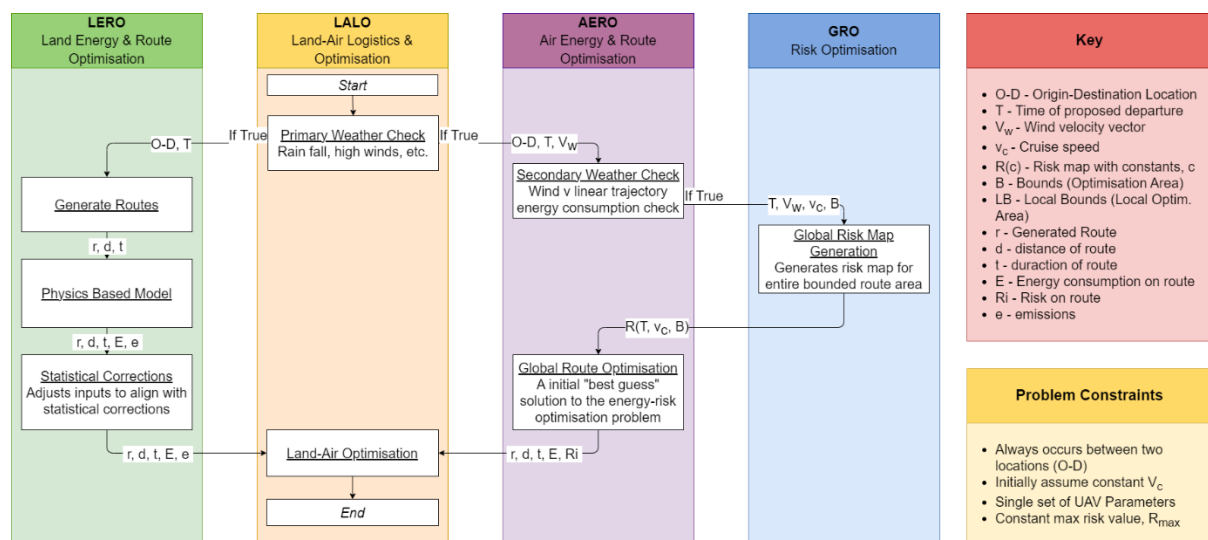


Figure 1. An overview of the FORSETI framework, broken down into the four main sections and highlighting the key parameters and problem constraints.

3 LAND-ENERGY ROUTING OPTIMISER (LERO)

This section describes the methodology of estimating travel time, energy consumption and emissions for land logistics. The assumed definition of land logistics encompasses diesel vans, electric vans and pedal bikes. The work presented in this chapter has been published by Krol *et al.* (2023).

In assessing the energy consumption of diesel and electric vans, modelling first employs a physics-based model assuming constant speed. This initial calculation is subsequently refined using a statistical model derived from historical data. Both diesel and electric vans undergo a similar process, albeit with distinct physics models and forms of statistical corrections.

The chosen physics-based models for this analysis are the Comprehensive Modal Emission Model (CMEM) for diesel vans and the Comprehensive Power-based EV Energy Consumption Model (CPEM) for electric vans. To determine the appropriate form of statistical adjustment, a Gaussian Process Regression is utilised. To construct this adjustment, both CMEM and CPEM are applied to historical driving cycles on an instantaneous basis and compared to instances where the instantaneous speed is set to the mean velocity. The analysis incorporates a comprehensive dataset of 14,984 driving cycles, representing diverse traffic states ranging from highway to urban driving. These data, sourced from various regions in the United States, were collated by the National Renewable Energy Laboratory.

The model's validity was verified using data collected from van journeys between different medical facilities in the Solent Region, located in the southwestern part of the United Kingdom. These locations simulate real-life logistics scenarios, with medical samples being transported to Southampton General Hospital for analysis.

The logistics model includes a built-in emissions model for estimating the emissions produced by electric and diesel vans. The pollutants¹ considered are carbon dioxide equivalent¹ (CO₂e), carbon dioxide (CO₂), oxides of nitrogen (NO_x) and particulate matter (PM₁₀). Pollutants are calculated using emissions factors (EFs) produced by the UK government. Emissions associated with climate change (CO₂e and CO₂) are calculated using EFs related to vehicle energy and fuel consumption (BEIS & DEFRA

¹ Total CO₂e for all species of greenhouse gases (GHGs) emitted, where CO₂e is the amount of CO₂ emitted that would cause the same time-integrated radiative forcing, over a given time-horizon, as an emitted amount of other GHGs.

2022) (Table 1). Emissions associated with detrimental effects on air quality (NO_x and PM₁₀) are calculated using EFs related to vehicle average speed and distance travelled (DfT 2023) (Table 2).

For climate change pollutants, the two components of Well-To-Wheel (WTW; i.e., total) emissions are calculated: i) Well-To-Tank (WTT) emissions associated with fuel production, processing and distribution; and ii) Tank-To-Wheel (TTW) emissions associated with fuel used in-vehicle. The terms WTT and TTW are more properly appropriate for liquid fuels (e.g., diesel), and so WTT-equivalent (WTTe) and TTW-equivalent (TTWe) have been adopted for electric vans. WTTe describes emissions associated with extraction, refining and transport of primary fuels before use in electricity generation and with losses in electricity transmission and distribution. TTWe describes emissions from generating the electricity used in-vehicle.

Air quality pollutants are a concern when emitted in proximity to sensitive receptors (i.e., humans), such as when emitted from the tailpipes of road vehicles (Uherek *et al.* 2010; Smit *et al.* 2008). Therefore, for NO_x and PM₁₀, only tailpipe (i.e., TTW) emissions from diesel vans are calculated (electric vans are assumed to not produce tailpipe emissions of these pollutants).

Table 1. Emission factors for CO₂e and CO₂ based on energy and fuel consumption (BEIS & DEFRA 2022).

CO ₂ e Emissions	EF	CO ₂ Emissions	EF
CO ₂ e WTTe	0.0505 kg CO ₂ e/kWh	CO ₂ WTTe	0.0499 kg CO ₂ /kWh
CO ₂ e WTT	0.6099 kg CO ₂ e/L	CO ₂ WTT	0.6010 kg CO ₂ /L
CO ₂ e TTWe	0.1934 kg CO ₂ e/kWh	CO ₂ TTWe	0.1912 kg CO ₂ /kWh
CO ₂ e TTW	2.5578 kg CO ₂ e/L	CO ₂ TTW	2.5206 kg CO ₂ /L

Notes: WTTe is Well-To-Tank-equivalent; WTT is Well-To-Tank; TTWe is Tank-To-Wheel-equivalent; TTW is Tank-To-Wheel.

Table 2. Average speed emission model coefficients for NO_x and PM₁₀ tailpipe emissions from diesel vans (DfT 2023).

EF (g/km)	a	b	c	d	E	f	g	Min. Speed (km/h)	Max. Speed (km/h)
NO _x	1.9E-02	2.5E-03	-5.5E-05	6.6E-07	-3.5E-09	2.4E-11	-6.9E-14	10	100
PM ₁₀	2.0E+00	4.6E-01	-5.1E-03	1.4E-04	-2.0E-06	1.4E-08	-7.6E-12	10	110

Average speed emission model format is $EF = (a + bv + cv^2 + dv^3 + ev^4 + fv^5 + gv^6)/v$; where v = vehicle average speed (km/h).

4 GROUND RISK OPTIMISER (GRO)

This section summarises the approaches and methods for quantifying and mapping the third-party risk (TPR) posed by UAS to uninvolved persons on the ground, in the vicinity of overflight. The model is fully parameterised and applicable to a wide variety of aircraft. The approach encompasses all four relevant dimensions, that is, three spatial dimensions and a temporal dimension, and is therefore highly specific to the operation at hand, aiming to provide the most accurate representation of ground risk. There are several steps involved in the procedure and the work has been published in Oakey *et al.* (2022) and Pilko *et al.* (2023).

4.1 Spatiotemporal Population Mapping

This work estimates actual population distributions from the highest resolution authoritative source available, namely census data. Whilst this is likely better than a uniform value being set for population density over large areas, this approach can still result in overestimation of the risk posed in urban areas due to the loss of resolution caused by using real data. The approach presented here is therefore more suited to longer BVLOS operations outside and around urban areas. The decision to use generic national data sources instead of attempting to concatenate many local datasets, which may have offered finer detail, was made to allow the approach to have a wide spatial applicability.

Estimates for dynamic populations derive from daily workflows segregated by demographic categories, for example school children or the elderly, which are mapped to their expected spatial locations for a given time. In this case, data from the census detailing the residential population is assumed to form 100% of the available population and is constant for a given area. The population categories are mapped to locations from human activity pattern studies to find the proportions of the population located in each of 10 different locations at a given time of day. The temporal population proportions must then be located spatially; this requires combination with geospatial geometries appropriate to the activity. The residential population in a given area is an estimate from a combination of census, OpenStreetMap (OSM) and National Human Activity Pattern Survey (NHAPS) data. The population density of each census area is found from the census data, as shown in Figure 2.

The population density value for each area is then scaled according to the proportion of the population that is located in residential locations for a given time of day. This ensures the population spatial distribution remains the same compared to the census data. There is no generally available counterpart to the census for non-residential areas that could be used to determine population densities for such areas on a large scale. Whilst it is possible to find building maximum occupancy data

for a smaller collection of buildings, this approach does not scale well to larger or different areas, requiring a large amount of manual data input and subsequent updating.

Firstly, the total population must be found. As previously discussed, taking the census data to form the total population is suitable. Secondly, the total population value is scaled by the proportions of the population for each location, to find the absolute values for the population in each of the locations. Next, the geospatial geometries of each location are found using data from OSM. The area for each of these geometries is calculated and summed together for all geometries associated with a given location. This is repeated for each location. The population and spatial data are then combined to a population density by dividing the absolute population value for each location by the total area for that location.

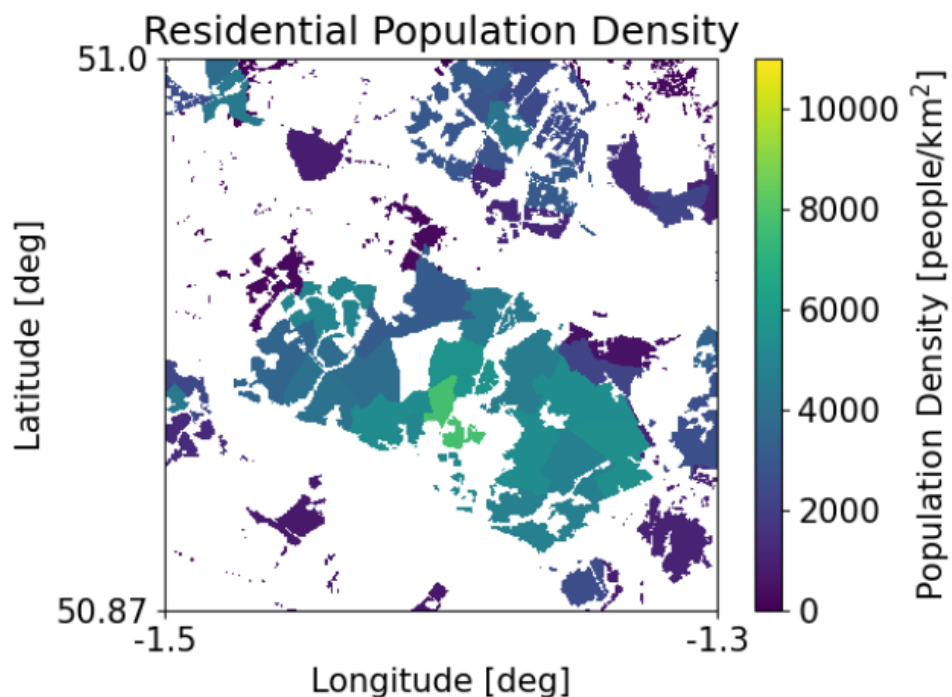


Figure 2. Residential Population map for the Southampton area. This shows the maximum density each residential area can have.

The road traffic population is derived from historical road traffic and vehicle occupancy estimates. It is used in combination with assumptions about the road geometry to derive the density of people located on any given location along a road. Historical road traffic is derived from open governmental data provided by the United Kingdom Department for Transport in the form of Annual Average Daily Flow (AADF) tables. AADF tables are produced by a combination of automatic traffic counters and manual enumeration of vehicles at a given point of on the road network.

The data used in this work uses the amalgamated traffic direction version, with counts categorized by vehicular type. AADF values are scaled by similarly provided values corresponding to hours of the day in order to obtain estimates for traffic flow for an average day in the year. Algorithm TKTK is based on the projection of each road geometry to a single dimension, followed by the superposition of traffic counter locations on the line according to distance along the road. The counter values are then interpolated between and projected back onto the original road geometry. This is used to generate a population density value for each section of road considered. Figure 3 demonstrates the large temporal variation in road population density for the same area at different times. This is calculated using Algorithm 1.

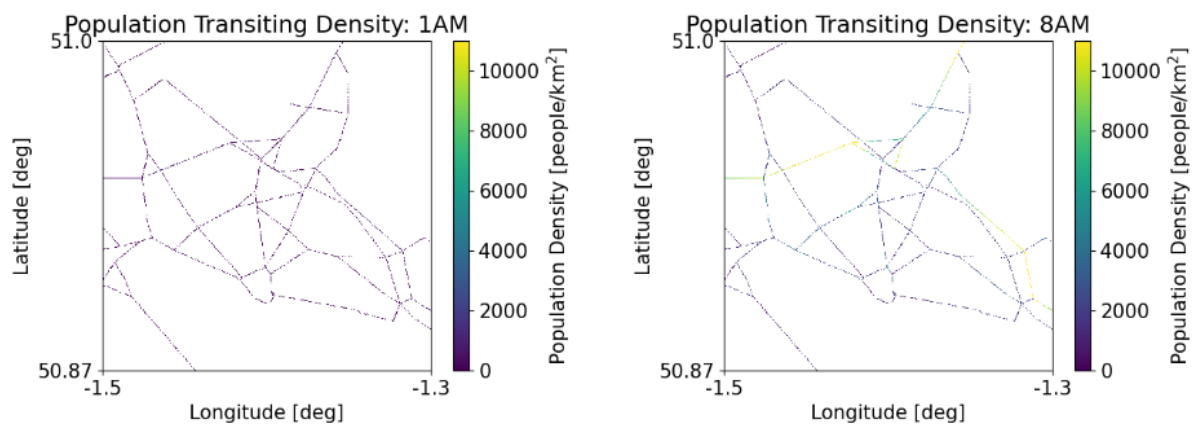


Figure 3. Roads population density at around Southampton, UK. Left shows a quiet period during the night, right shows a “rush hour” traffic period.

Algorithm 1. Calculation of road population density.

Input: unique road identifiers L ; road geometry line segments S ; traffic counter populations T ; interpolation resolution r ;
Result: a set of 2-tuples of georeferenced polygons and associated population density values P

```

1 for  $\forall l \in L$  do
2    $S_l \leftarrow \text{GetSegmentsForRoad}(S, l)$ ;
3    $T_l \leftarrow \text{GetCountersForRoad}(T, l)$ ;
4    $O \leftarrow \emptyset$ ;
5   for  $\forall s \in S_l$  do
6      $T_s \leftarrow \text{GetCountersOnSegment}(T_l, s)$ ;
7      $carriedLength := 0$ ;
8     if  $T_s \neq \emptyset$  then
9        $O \leftarrow O \prec (\text{Length}(s) + carriedLength)$ ;
10       $carriedLength := 0$ ;
11    else
12       $carriedLength += \text{length}(s)$ ;
13    end
14  end
15   $nPoints \leftarrow \lfloor \text{Max}(O)/r \rfloor$ ;
16   $M_l \leftarrow \text{Interpolate}(O, T_l, nPoints)$ ;
17   $w \leftarrow \text{GetRoadWidth}(l)$ ;
18   $R_l \leftarrow \text{Buffer}(S_l, w)$ ;
19  for  $\forall i \in \{0, 1, 2, \dots, nPoints\}$  do
20     $clippedPolygon \leftarrow \text{Buffer}(\text{GetLatLng}(O_i), r/2) \cap R_l$ ;
21     $P \leftarrow P \prec \{clippedPolygon, M_{l,i}/\text{Area}(clippedPolygon)\}$ ;
22  end
23 end

```

4.2 Flight Path Ground Risk Analysis

The probabilistic approach taken to analyse the risk posed to people on the ground by a UAS is widely used in previous work. It is based on the sequential occurrence of independent events, each with associated probabilities. The events, in order of occurrence, are:

1. Loss of Control (LoC) event that results in the UAS impacting the ground
2. Striking a person(s) as a result of the uncontrolled descent
3. The struck person(s) being fatally injured as a result

Previous models are subsequently extended with the addition of time-based quantities:

$$P_{\text{casualty}}(x, y, t) = P_{\text{LoC}} \cdot P_{\text{strike}}(x, y, t) \cdot P_{\text{fatality}}(x, y)$$

where x and y refer to the spatial dimensions, t is hour of the day. The hour of the day t is used to as input to the spatiotemporal population density model.

4.2.1 Probability of Striking Persons

The probability of striking a person, P_{strike} , given an impact of a UAS at a position x, y and time t is

$$P_{\text{strike}}(x, y, t) = \sum_{x,y} PDF \cdot \rho(x, y, t) \cdot A_{\text{exp}}(\theta)$$

Where ρ is the population density; A_{exp} is the lethal area for the impact angle θ . The lethal area is found by:

$$A_{exp} = \frac{2h_{person}(r_{person} + r_{uas})}{\tan \theta} + \pi(r_{person} + r_{uas})^2$$

Where the height of a person, h_{person} , is assumed to be 1.8m, the radius of a human, r_{person} is assumed to be 1.0m and the aircraft radius, r_{uas} , is set to half the maximum dimension of the aircraft considered.

4.2.2 Probability of Fatality

The fatality model used here was proposed by Dalamagkidis *et al.* (2008) and is based upon a logistic growth model as shown in Figure 4. The curve is defined by:

$$P_{fatality}(x, y) = \frac{1}{1 + \sqrt{\frac{\alpha}{\beta}} \left[\frac{\beta}{E_K^{imp}(x, y)} \right]^{\frac{1}{S(x, y)}}}$$

where $E_K^{imp}(x, y)$ is the impact kinetic energy, α is the impact energy required for 50% probability of fatality at a shelter factor $S = 0.5$ and β is minimum impact energy to cause a fatality with no shelter ($S \rightarrow 0$). The shelter factor $S(x, y)$ is in the interval $[0, 1]$ and encompasses shelter effects that obstacles in the vicinity of the impact (e.g., buildings, vehicles) have both in terms of blocking the path of the UAS, resulting in it not striking a person, and absorbing impact energy. In this work, the sheltering factor is set to 0.3 as a conservative average value with more detailed sheltering maps left to future work.

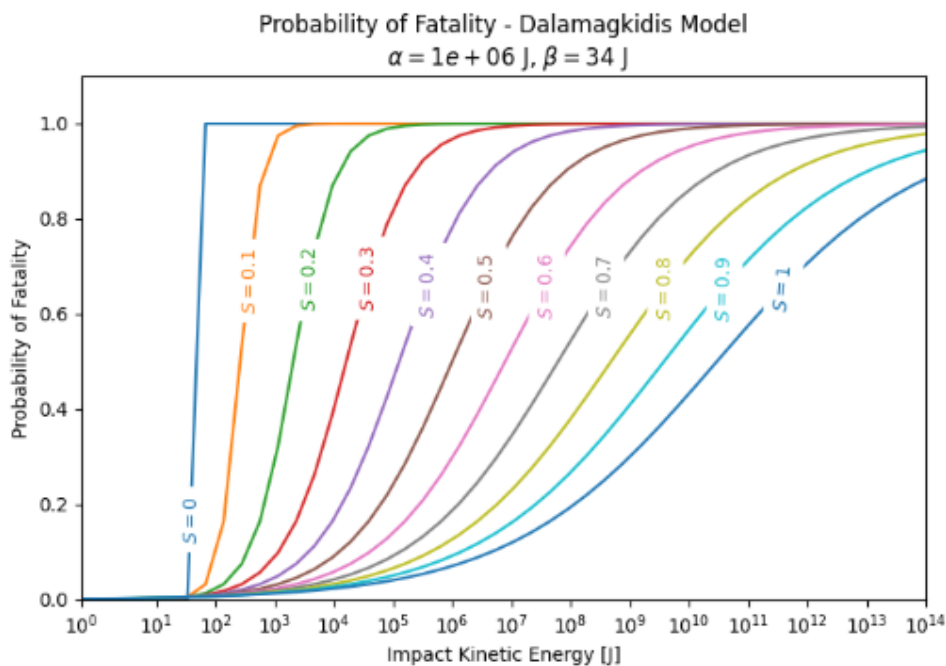


Figure 4. Fatality Curves created from the model by Dalamagkidis *et al.* (2008).

4.3 Mapping of Ground Risk

A region encompassing Southampton, UK is used as an example; a satellite view of the region is seen in Figure 5. The upper right of this view also shows Southampton Airport which is only considered later through the addition of the corresponding Flight Restriction Zone for UAS around it.

The population density maps generated demonstrate a marked redistribution of population throughout the day with residential areas almost regaining their full populations as defined in the census data during night-time hours, shown in Figure 6. Conversely, daylight hours demonstrate a shift toward industrial, commercial, public and retail areas as people relocate to workplaces and engage in commerce. The final ground risk maps can be seen at various times of the day for the same region as the population maps. Figure 7 and Figure 8 show the strike and fatality risk respectively for the Swoop Aero Kookaburra aircraft at 120m above ground.



Figure 5. Southampton region used throughout this paper for demonstration (Maps © Google, 2023).

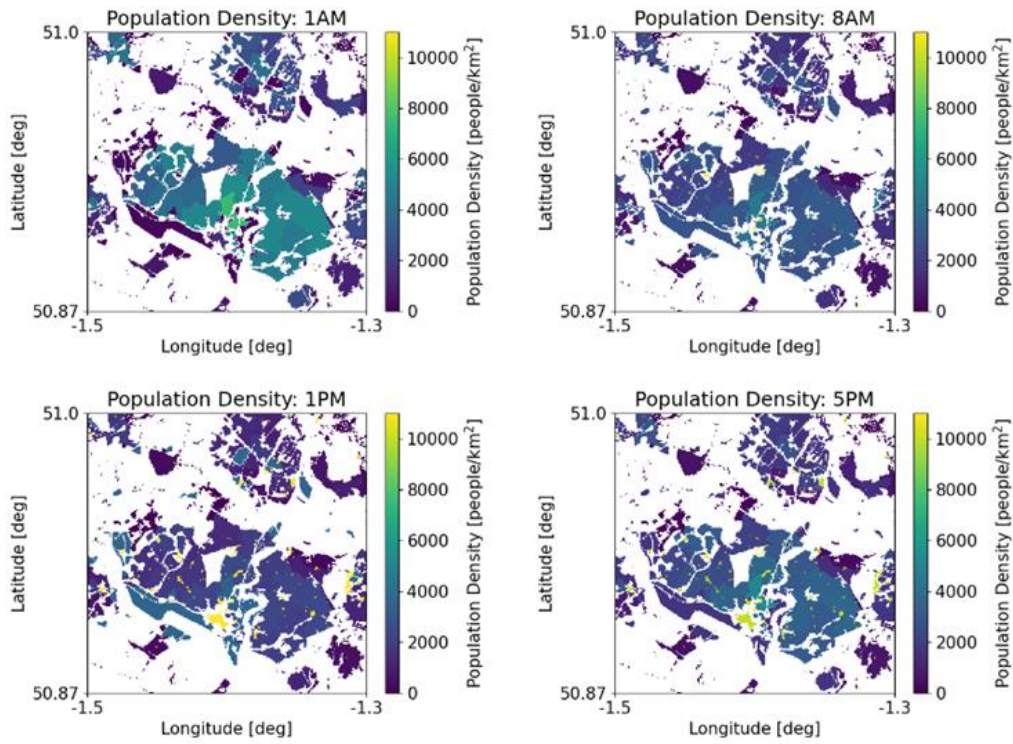


Figure 6. Comparison of population densities at different times of the day around Southampton, UK

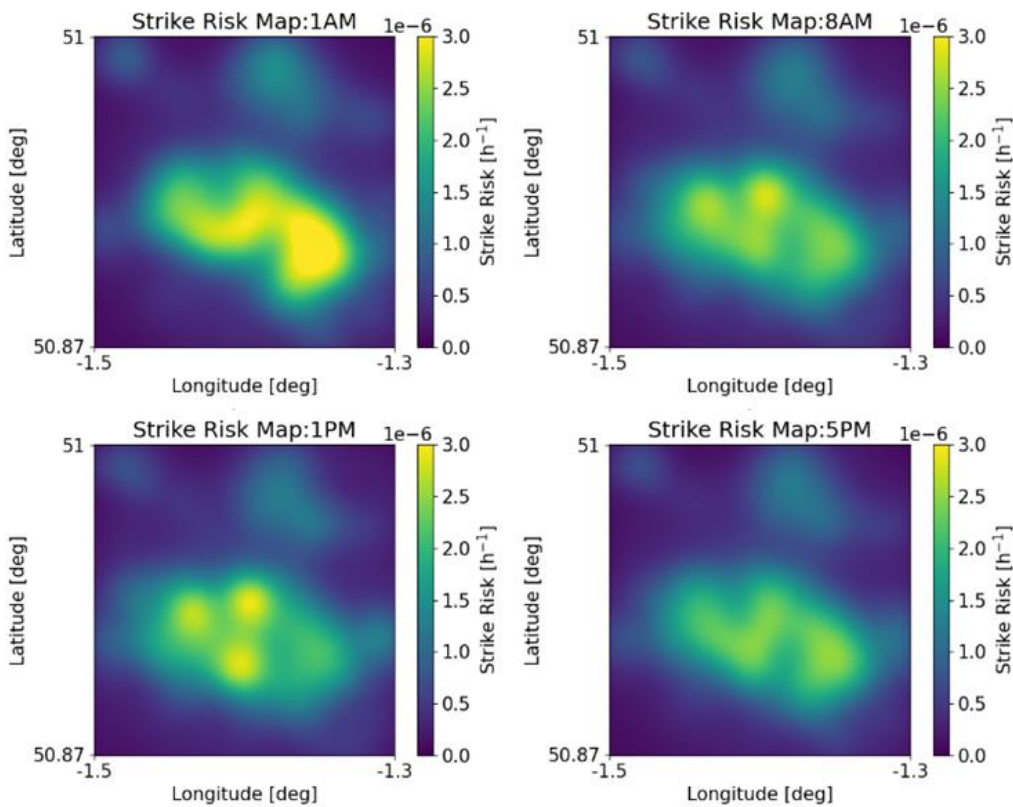


Figure 7. Comparison of strike risk maps at different times of the day around Southampton, UK. Swoop Aero aircraft used at a height of 120m.

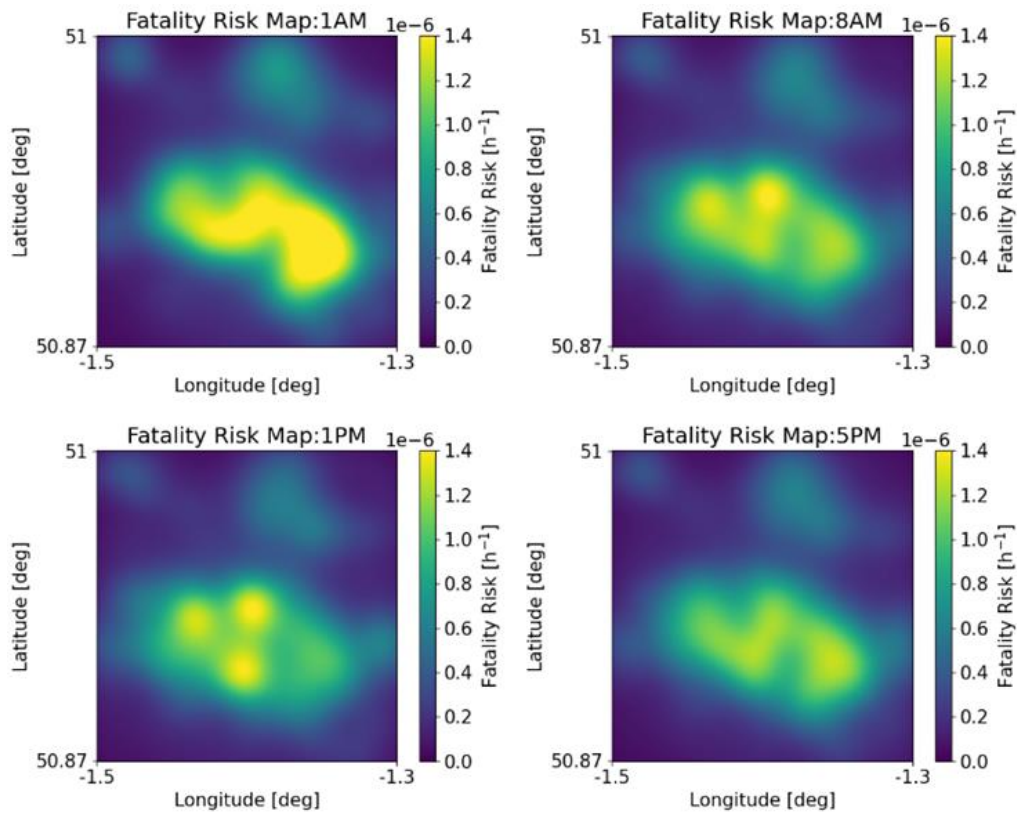


Figure 8. Comparison of fatality risk maps at different times of the day around Southampton, UK. Swoop Aero aircraft used at a height of 120m.

5 AIR ENERGY ROUTE OPTIMISER (AERO)

This section explores the methodology used to generate routes for a UAV through a 3D space that are dynamically feasible and energy minimal. There are a series of components that must be defined to effectively achieve this, including the energy consumption model, the dynamic equations of motion of the UAV, the state space which the drone can operate in, the control vector of the UAV and any other constraints that may act on the drone. Each of these components are separately explored in this section. The work presented has been published by Blakesley *et al.* (2022).

5.1 Energy Consumption Modelling

In order to achieve minimum energy routes between two locations in a 3D space, a model for the energy consumption of a UAV needs to be defined and then minimised within an objective function. To compute the energy consumption in the objective function without excessive computational demands (and thus avoid long run times), an estimation is used to find the energy consumption during route optimisation. The estimation of the objective function is given by:

$$E = \int_{t_0}^{t_f} \sum_{i=1}^4 \omega_i t^3 dt$$

Where ω is the angular velocity of the rotor blades for the i th motor. This is then minimised throughout the optimisation by the objective function, given by

$$\min_{\omega_i} E$$

Once the trajectory has been identified, a more detailed model is used to find the exact energy consumption. The instantaneous energy, E_i , associated with the i -th motor is evaluated following an approach in [9], given by

$$\begin{aligned} E_i = & \frac{RT_f^2}{K_T^2} + \frac{T_f}{K_T} \left(\frac{2RD_f}{K_T} + K_T \right) \omega_i(t) \\ & + \left(\frac{D_f}{K_T} \left(\frac{RD_f}{K_T} + K_T \right) + \frac{2RT_f k_\tau}{K_T^2} \right) \omega_i^2(t) \\ & + \frac{k_\tau}{K_T} \left(\frac{2RD_f}{K_T} + K_T \right) \omega_i^3(t) \\ & + \frac{Rk_\tau^2}{K_T^2} \omega_i^4(t) \\ & + \frac{RJ^2}{K_T^2} \dot{\omega}_i^2(t), \end{aligned}$$

where K_T is the motor torque constant, K_v is the motor velocity constant, T_f is the motor friction torque, D_f is the motor viscous damping coefficient and R is the resistance of phase winding.

5.2 Dynamic Equations of Motion

The dynamic equations are applied as a constraint to the problem to ensure that the UAV flies realistically throughout the trajectory. These equations are formulated as a series of force balancing equations in the x , y , z directions, moment balancing equations around the body co-ordinate frame and auxiliary equations to convert between the first and second order differential equations systems. These are given by

$$\begin{aligned} \dot{x} &= \frac{ax}{dt}, \\ \ddot{x} &= \frac{T}{m}(\cos \phi \sin \theta \cos \psi + \sin \phi \sin \psi) - F_D(\dot{x}), \\ \dot{y} &= \frac{dy}{dt}, \\ \ddot{y} &= \frac{T}{m}(\cos \phi \sin \theta \sin \psi - \sin \phi \cos \psi) - F_D(\dot{y}), \\ \dot{z} &= \frac{dz}{dt}, \\ \ddot{z} &= \frac{T}{m}(\cos \phi \cos \theta) - g \left(\frac{2}{1 + e^{-k\|\Delta \mathbf{x}\|^2}} - 1 \right), \\ \dot{\phi} &= \frac{d\phi}{dt}, \\ \ddot{\phi} &= \frac{I_y - I_z}{I_x} \dot{\theta} \dot{\psi} + \frac{(F_2 - F_4)l}{I_x} - \frac{J\dot{\theta}\bar{\omega}}{I_x}, \\ \dot{\theta} &= \frac{d\theta}{dt}, \\ \ddot{\theta} &= \frac{I_z - I_x}{I_y} \dot{\phi} \dot{\psi} + \frac{(F_3 - F_1)l}{I_y} + \frac{J\dot{\phi}\bar{\omega}}{I_y}, \\ \dot{\psi} &= \frac{d\psi}{dt}, \\ \ddot{\psi} &= \frac{I_x - I_y}{I_z} \dot{\phi} \dot{\theta} + \frac{(M_1 - M_2 + M_3 - M_4)}{I_z}, \end{aligned}$$

Where all variables are given in Table 3.

Table 3. Variables used in the air energy route optimisation tool.

Panel A: Parameter values independent of drone		
Variable	Symbol	Units
Air density	ρ	kg/m ³
Acceleration due to gravity	g	m/s ²
Panel B: Static parameter values dependent on drone		
Number of rotor blades	n_B	-
Blade to motor hub offset	ϵ	m
Mass of a blade	m_B	kg
Radius of the propeller	r	m
Drone arm length	l	m
Mass of drone body	m	kg
Drone body drag coefficient	C_D	-
Propeller thrust coefficient	C_T	-
Propeller torque coefficient	C_Q	-
Projected area of drone body	A_f	m ²
Rotor moment of inertia	J_m	kgm ²
X component of body inertia	I_x	kgm ²
Y component of body inertia	I_y	kgm ²
Z component of body inertia	I_z	kgm ²
Rotor velocity constant	K_V	rpm/V
Rotor torque constant	K_T	Vs/rad
Rotor friction torque	T_f	Nm
Viscous damping coefficient	D_f	Nms/rad
Phase winding resistance	R	Ω
Maximum angular velocity	ω_{max}	rad/s
Landing scaling factor	k_e	-
Landing distance factor	k_d	-
Panel C: Dynamic parameter values describing the drone		
Position in x, y, z	x, y, z	m
Velocity in x, y, z	$\dot{x}, \dot{y}, \dot{z}$	m/s
Acceleration in x, y, z	$\ddot{x}, \ddot{y}, \ddot{z}$	m/s ²
Drone roll, pitch, yaw	ϕ, θ, ψ	rad
Roll, pitch, yaw velocity	$\dot{\phi}, \dot{\theta}, \dot{\psi}$	rad/s
Roll, pitch, yaw acceleration	$\ddot{\phi}, \ddot{\theta}, \ddot{\psi}$	rad/s ²
Rotor angular velocity	ω_i	rad/s

5.3 State, Control Vectors and Bounds

The state space consists of a UAV's position (x, y, z) relative to the earth frame and rotation (ϕ, θ, ψ) around the body frame in the x, y, z directions, as well as their rates of change over time, i.e.

$$X = [x, y, z, \phi, \theta, \psi, \dot{x}, \dot{y}, \dot{z}, \dot{\phi}, \dot{\theta}, \dot{\psi}]^T,$$

and the control vector consists of the angular velocity, ω , of the four motors of the quadcopter, i.e.

$$U = [\omega_1, \omega_2, \omega_3, \omega_4]^T.$$

A series of bounds are also applied to the problem to reduce the size of the state space and to ensure the drone flies realistically. These are given by

$$0 \leq \omega_i \leq \omega_{max},$$

$$0 \leq z,$$

$$\phi_{min} \leq \phi \leq \phi_{max},$$

$$\theta_{min} \leq \theta \leq \theta_{max}.$$

6 COMBINED AIR RISK-ENERGY TRAJECTORY OPTIMISER

In order to include risk as well as energy in the route optimisation framework, a second term is added to the objective function. This term queries the risk map at the locations along the trajectory in order to find the value of the cumulative risk, R , over the course of the trajectory. The objective function becomes:

$$\min_{\omega_i} \alpha R + (1 - \alpha)E.$$

The optimiser then finds an optimal route by minimising the objective function. The result for a flight between Southampton General Hospital and Hythe Hospital can be seen in Figure 9.

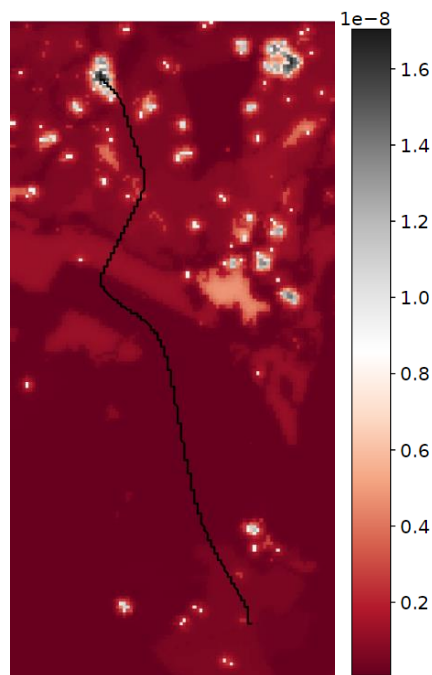


Figure 9. A minimum energy and risk route generated by the AERO and GRO sections of the FORSETI framework between Southampton General Hospital and Hythe Hospital. The risk is given by a colour map and a black line is overlaid to show the travelled trajectory of the UAV.

7 LAND-AIR LOGISTICS OPTIMISER (LALO)

After collating the OD pair data (see previous sections), LALO is then used to identify the best combination of routes to use for a given objective. The work presented in this section has been published in Oakey *et al.* (2022) and Oakey *et al.* (2023).

Modelling considers vans to operate in rounds of any number of stops, serving any site; drones operating to single sites (due to capacity and regulatory constraints), serving only those that are deemed drone suitable in the input scenario (e.g., Figure 10); and bikes serving up to 4 sites (due to capacity constraints), serving only those that are deemed cycle accessible in the input scenario (Figure 11). Range and time constraints can also be applied to the individual routes, as required.



Figure 10. Drone landing site space can influence the suitability of sites for drone service. Note: featured exclusion zone is a relaxation on existing regulations.

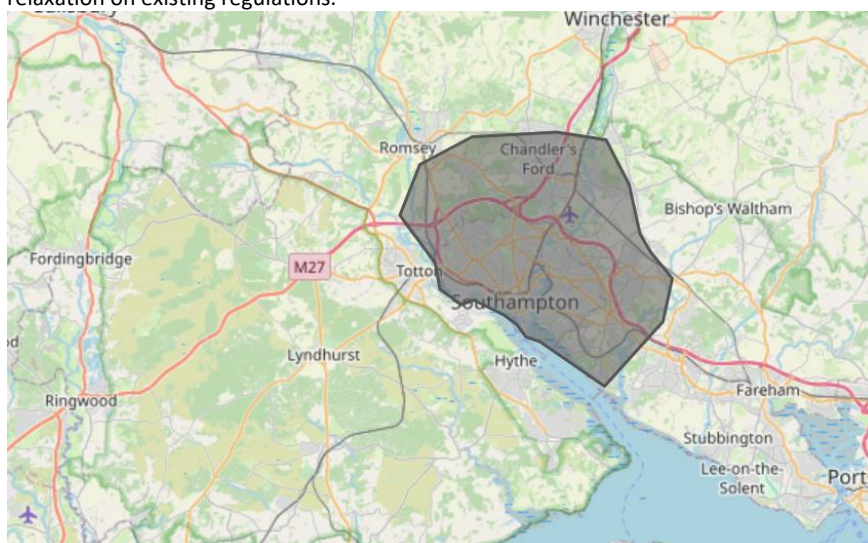


Figure 11. Area with available gig-economy cyclists in the Southampton area.

The LALO model is constructed with the movement of NHS diagnostic specimens from community clinics (GP surgeries) to a hospital laboratory for analysis. Current operations use diesel vans that complete scheduled vehicle rounds, serving multiple surgeries before each return to the delivery point. In the proposed system, routes are designed to work in combination, with cyclists and some vans being based at local clinics, completing local consolidation to local clinics; meanwhile, drones and the majority of vans are based at the hospital, serving the consolidation sites and others that fall out of the range of consolidation (Figure 12).

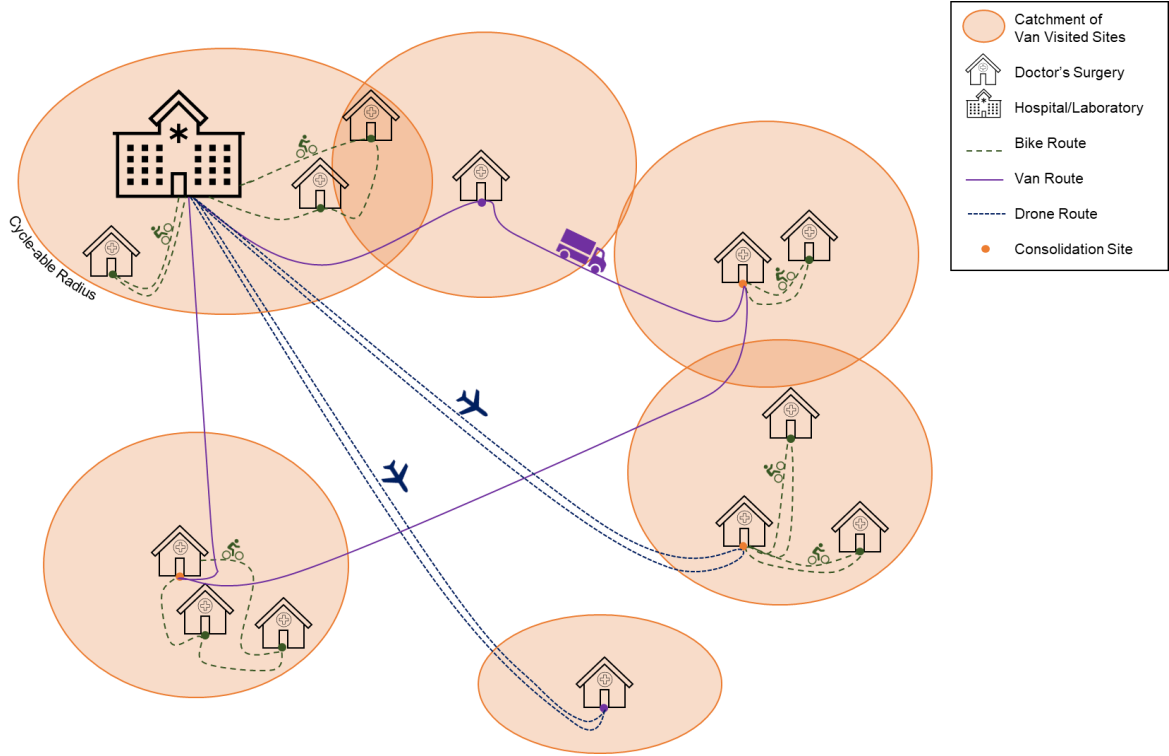


Figure 12. Schematic of operating strategy

The model aims to optimise a weighted objective function, balancing a combination of (i) the operating costs of the system (p and W values in below equation); (ii) the maximum transit time across the system (u value in below equation); (iii) the energy/emissions of the system (ϵ value in equation below) (Figure 13). The full formulation is given in Chapter 6 of Oakey (2023). The weights (θ values) can be defined according to the users' objective requirements.

$$\begin{aligned} \min : & \sum_{\bar{r}_k \in \bar{R}} \left(x_{\bar{r}_k} \left(\sum_{r_{v,k} \in \bar{r}_k \cap R^V} \theta_1 p_{r_{v,k}} + \sum_{r_{e,k} \in \bar{r}_k \cap R^E} \theta_1 p_{r_{e,k}} \right. \right. \\ & \left. \left. + \sum_{r_{d,k} \in \bar{r}_k \cap R^D} \theta_2 p_{r_{d,k}} + \sum_{r_{c,k} \in \bar{r}_k \cap R^C} \theta_3 p_{r_{c,k}} + \theta_4 \epsilon_{\bar{r}_k} \gamma \right) \right) \\ & + \theta_1 W^V A_{max}^V \\ & + \theta_2 (W^D A_{max}^D + W^O A_{max}^O) \\ & + \theta_5 u \end{aligned}$$

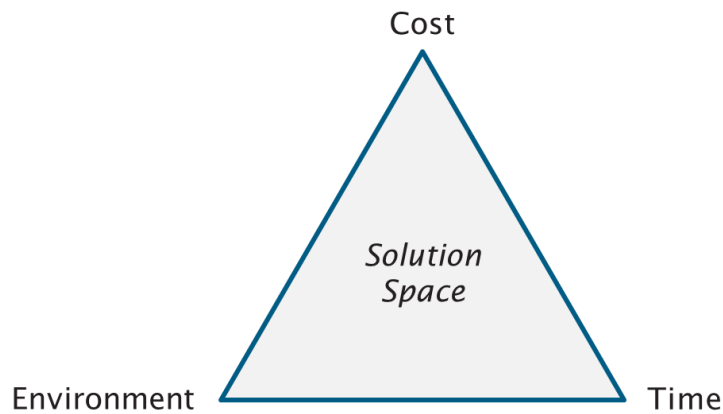


Figure 13. Solution space covered by the objective function

Other objectives, such as third-party risk, the number of vehicles, or total driving time can also be considered in modelling, though were not so relevant in the medical use case studied.

The model splits operations into shift periods of a few hours (as defined by the user), where every site is served once per period. Cost structures are based on typical operations, assuming drivers and remote drone operators are paid for a full shift period if they are assigned any routes; thus, the maximum number of each mode used at any point defines the fixed costs (Figure 14).

In the case of drones, operators can also manage more than 1 drone each, depending on the drone:operator ratio. In modelling, a 1:20 ratio was used; thus, 1 operator would be required for 1 drone, whilst 1 operator would also be required for 15 drones.

Time Point	1	2	3	4	5	6	7	8	...	k
Van 1	█	█	█	█			█	█	█	█
Van 2		█	█	█	█			█	█	█
Van 3			█	█	█	█				
# In Use	1	2	3	3	2	1	1	2	2	2

Figure 14. The number of van drivers required is defined by the maximum number in use at any time point.

Both drone and van costs are broken into a fixed cost, based on the number of vehicles/operators required in each shift; and the sum of the route costs, based on a distance-based metric (vans) or a time-based metric (drones, per flight hour) that depend on the variable costs such as parts and maintenance or fuel. The per flight hour approach aligns with typical flight maintenance scheduling used in crewed aviation to guarantee airworthiness (CAA 2022).

Cyclists are assumed to operate on a gig-economy style structure, where riders are used on demand and are paid subject to a fee per route, with supplementary fees for longer distances and additional stops. It should be highlighted that there are challenges associated with the gig-economy model, though for the purposes of modelling, this approach is sufficient to demonstrate the effects of cycling. Further details on the modelled costs and typical values are provided later in this document.

The transit time objective is given by the maximum time samples spend in transit across all sites. i.e., the longest period between the first collection and subsequent delivery in a route, for all routes. This value represents the timeliness of deliveries, with the transit time being the most easily and reliably influenced factor that can be changed by logistics planners to improve service quality in this sector (McDonald 1972). To this end, minimising the maximum time was chosen to encourage service equity across an area, in a similar manner to ambulances, as opposed to using an average, where times could be unevenly skewed.

To guarantee a given level of service, transit times can also be subject to a limit. In modelling, both (i) no limit, and (ii) a limit of 90 minutes (based on proposed targets in literature (McDonald 1972)) were explored. With respect to individual stops, a uniform dwell time was used across all stops and modes. In the modelling this was 2.5 minutes to allow for tasks such as loading/unloading and transporting the packages to/from the clinics. On return to the hospital, drones were subject to a further downtime period (10 minutes in modelled cases) to allow for battery changes and airworthiness checks.

Finally, to limit the data requirements, OD pair data are captured on an hourly basis and scaled for travel times between these periods. i.e., a 30-minute journey between two sites at 09:45 would be scaled using the travel time from 09:00 and 10:00.

To solve the model, an adapted Clarke and Wright Savings Algorithm with adapted bin packing algorithms are used. This provides effective solutions in a relatively short space of time, allowing for planning of operations in a short period prior to the shifts commencing for maximum foresight of weather and traffic conditions, and the required collections for the day. For more detail on heuristic solution approach methodology, please refer to Chapter 6/7 in Oakey (2023).

7.1 Van Cost Values

Suggested values for diesel van costs (Table 4) were obtained from the Manager's Guide to Distribution Costs (MGDC) published in the UK by the Freight Transport Association (FTA).

Table 4. Diesel van cost values.

Van Cost Input	Value (FTA 2020)	Value (FTA 2022)
Per Mile	£9,346/35,000mi = £0.27/mi	£12,254/36,000mi = £0.34/mi
Per Hour (Labour)	£10.78/h	£11.93/h
Per Vehicle Per Day	(£5,255+£1,639)/252 days = £27.36/veh./day	(£5,338+£2,054)/252 = £29.33/veh./day

FTA is the Freight Transport Association. Number of working days in a year (excluding eight Bank Holidays) is 252.

7.2 Bicycle Courier Cost Values

Bike courier cost values were based on the prices charged in the UK by a real-world bike courier company (Stuart Couriers, a provider of independent bicycle, motorcycle and car couriers in several European countries, <https://couriers.stuart.com/>). Within Stuart served areas (i.e., geographic areas where Stuart couriers are operational), prices charged by Stuart (available via online queries) are used to calculate the actual costs of each bike courier journey.

If Stuart areas are selected, then only collection locations within the Stuart area will be considered for servicing by bike (as long as the bike option has been selected for a particular location by the user). Collection locations outside the Stuart area will not be serviced by bike (regardless of whether or not the user has the bike option selected for a particular location). If Stuart areas are selected off, all collection locations with the bike option selected by the user will be considered for servicing by bike, and default bike costs will be used. Suggested values for these default bike costs (Table 5) were derived from an analysis of Stuart prices for a given sample of different bike courier journeys.

Table 5. Bicycle courier default cost values.

Bike Courier Cost Input	Value
Per Mile	£1.01/mi
Per Mile Threshold	0.5 mi
Per Task	£7.07/task
Per Stop	£2.78/stop

Regarding Table 5, a task was defined as one bike courier journey making collections from one or more collection locations for one delivery, all at the same delivery location. Additional stops were defined

as the number of extra collection locations in addition to the first collection location on a particular courier journey. Threshold distance was defined as the distance beyond which couriers are paid the additional mileage rate (i.e., Cost 1). For example, one courier journey of 2.5 miles involving two collections would cost $(1 \text{ task} \times \text{£}7.07/\text{task}) + (1 \text{ additional stop} \times \text{£}2.78/\text{additional stop}) + (2.0 \text{ mi} \times \text{£}1.01/\text{mi}) = \text{£}11.87$.

7.3 Drone Cost Values

Suggested values for drone costs (Table 6) were derived from a combination of: literature sources, commercially available data, and the drone expertise possessed by members of the FORSETI development team and associated partners (<https://cascadeuav.com/>). The costs are related to four elements: i) life expectancy of drone components (e.g., airframe, motors, propellers, servos, autopilots, and communications equipment); ii) electrical energy consumption during different flight stages (e.g., take-off, cruise, landing); iii) personnel involved (e.g., operator (often known as mission commander), safety pilot, loader); and iv) operational insurance. The current values in Table 6 represent estimates for present-day costs (i.e., in 2023).

The potential future values in Table 6 represent estimates for drone costs in a future situation based on a reasonable assumption of increasing automation as drone logistics operations and technologies mature. Automation of operations was assumed to result in employment as a drone operator becoming a less skilled (and therefore lower paid) occupation, and for the requirements for safety pilots and loaders to be reduced or removed entirely. Drone platforms were assumed to be less costly in the future due to economies of scale resulting from the forecast expansion of the global drone industry.

Table 6. Drone cost values.

Drone Cost Input	Current Value	Potential Future Value
Per Hour (Labour)	£175.64/h (1x Operator at £50/h; 2x Safety Pilot at £50/h; 2x Loader at £10.26/h)	£31.44/h (1x Operator at £20.26/h; 0x Safety Pilot at £20.26/h; 1x Loader at £10.26/h)
Per Flight Hour (Vehicle)	£32.40/h (Drone platform; electricity)	£20.33/h (Drone platform; electricity)
Per Vehicle Per Day	£8.99/veh./day (Insurance; UTM fees)	£8.99/veh./day (Insurance; UTM fees)

Potential future values are provided in terms of the present value of the UK pound (2023) and would need to be adjusted for inflation if an estimate of projected future costs was required. A 3% profit margin for the drone service provider is included. UTM is UAV Traffic Management, and relates to the fees charged for managing airspace by UTM service providers.

The interaction between drone labour costs per hour and the operator-to-vehicle ratio set by the user (i.e., the number of drones that can be operated by a single operator at any one time) is best explained by way of an example based on the values in Table 6. If the operator ratio is set to ten (i.e., drone operators, plus safety pilots and loaders as per Table 6), then operating any number of drones from one to ten simultaneously will cost £175.64/h at current values (£31.44/h at potential future values), and operating any number of drones from 11 to 20 simultaneously will cost $2 \times £175.64/h = £351.28/h$ at current values ($2 \times £31.44/h = £62.88/h$ at potential future values). In other words, the services of one drone operator are required for any number of drones from 1 to 10, two drone operators are required simultaneously for any number of drones from 11 to 20, three drone operators for 21 to 30 drones, and so on.

8 CASE STUDY RESULTS

For case study results and the exact inputs used modelled in each of the experiments, please consult the following peer-reviewed literature:

- Oakey, A., Grote, M., Smith, A., Cherrett, T., Pilko, A., Dickinson, J., AitBihiOuali, L., 2022. Integrating drones into NHS patient diagnostic logistics systems: Flight or fantasy? PLOS ONE 17, e0264669. <https://doi.org/10.1371/journal.pone.0264669>
- Oakey, A., Martinez-Sykora, A., Cherrett, T., 2023. Improving the efficiency of patient diagnostic specimen collection with the aid of a multi-modal routing algorithm. Computers & Operations Research 106265. <https://doi.org/10.1016/j.cor.2023.106265>
- Grote M, Oakey A, Pilko A, Krol J, Blakesley A, Cherrett T, Scanlan J, Anvari B and Martinez-Sykora A (2023) 'The Effects of Costs on Drone Uptake in Multi-Modal Logistics Systems within a Healthcare Setting', *Transport Economics and Management* (under review).
- Oakey, A., 2023. Investigating the scope for integrating uncrewed aerial vehicles (UAVs) into mixed-mode fleets to support national health service (NHS) logistics operations (PhD Thesis). University of Southampton. <https://eprints.soton.ac.uk/483801/>

REFERENCES

- Blakesley A, Anvari B, Kroll J and Bell M G H. Minimum energy route optimisation of a quad-copter UAV with landing incentivisation. 2022 IEEE 25th International Conference on Intelligent Transportation Systems (ITSC), 8-12 October 2022, Macau, China. Institute of Electrical and Electronics Engineers (IEEE), 2300-2306.
- Civil Aviation Authority (CAA) (2022) *Unmanned Aircraft System Operations in UK Airspace - Policy and Guidance (CAP 722)*, Crawley, UK: Civil Aviation Authority.
- Dalamagkidis K, Valavanis K P and Piegł L A (2008) 'On unmanned aircraft systems issues, challenges and operational restrictions preventing integration into the National Airspace System', *Progress in Aerospace Sciences*, 44(7-8), 503-519.
- Department for Business Energy & Industrial Strategy (BEIS) and Department for Environment Food & Rural Affairs (DEFRA) (2022) *UK Government GHG Conversion Factors for Company Reporting*, London, UK: Department for Business, Energy & Industrial Strategy.
- Department for Transport (DfT) (2023) *WebTAG Data Book (January 2023)*, London, UK: Department for Transport.
- Freight Transport Association (FTA) (2020) *Manager's Guide to Distribution Costs*, Tunbridge Wells, UK: Freight Transport Association Limited.
- Freight Transport Association (FTA) (2022) *Manager's Guide to Distribution Costs - October 2022 Update Report*, Tunbridge Wells, UK: Freight Transport Association Limited.
- Krol J, Anvari B, Blakesley A and Cherrett T. Estimation of Energy Usage in Electric and Diesel Vans for Logistics Applications Using Gaussian Processes. Transportation Research Board (TRB) 102nd Annual Meeting, 8-12 January 2023, Washington D.C., USA. Transportation Research Board.
- McDonald J J (1972) 'Vehicle Scheduling - A Case Study', *Operational Research Quarterly*, 23(4), 433-444.
- Oakey A. (2023). *Investigating the scope for integrating uncrewed aerial vehicles (UAVs) into mixed-mode fleets to support national health service (NHS) logistics operations*. Thesis submitted for Doctor of Philosophy, University of Southampton.
- Oakey A, Grote M, Smith A, Cherrett T, Pilko A, Dickinson J and Ait Bihi Ouali L (2022) 'Integrating drones into NHS patient diagnostic logistics systems: Flight or fantasy?', *PLoS One*, 17(12), e0264669.
- Oakey A, Martinez-Sykora A and Cherrett T (2023) 'Improving the efficiency of patient diagnostic specimen collection with the aid of a multi-modal routing algorithm', *Computers & Operations Research*, 157.
- Pilko A, Sóbester A, Scanlan J P and Ferraro M (2023) 'Spatiotemporal Ground Risk Mapping for Uncrewed Aircraft Systems Operations', *Journal of Aerospace Information Systems*, 20(3), 126-139.
- Smit R, Brown A L and Chan Y C (2008) 'Do air pollution emissions and fuel consumption models for roadways include the effects of congestion in the roadway traffic flow?', *Environmental Modelling & Software*, 23(10-11), 1262-1270.

Uherek E, Halenka T, Borken-Kleefeld J, Balkanski Y, Berntsen T, Borrego C, Gauss M, Hoor P, Juda-Rezler K and Lelieveld J (2010) 'Transport impacts on atmosphere and climate: Land transport', *Atmospheric Environment*, 44(37), 4772-4816.